NMR Evidence for Syn-Anti Interconversion of a Trans Opened (10*R*)-dA Adduct of Benzo[*a*]pyrene (7*S*,8*R*)-Diol (9*R*,10*S*)-Epoxide in a DNA Duplex†

D. E. Volk,‡ J. S. Rice,‡,§ B. A. Luxon,‡ H. J. C. Yeh,|| C. Liang,|| G. Xie,|| J. M. Sayer,|| D. M. Jerina,|| and D. G. Gorenstein*,‡

Sealy Center for Structural Biology and Department of Human Biological Chemistry and Genetics, University of Texas Medical Branch, Galveston, Texas 77555-1157 and National Institute of Diabetes and Digestive and Kidney Diseases, The National Institutes of Health, Bethesda, Maryland 20892-0820

Received July 18, 2000; Revised Manuscript Received September 13, 2000

ABSTRACT: 2D NMR has been used to examine the structure and dynamics of a 12-mer DNA duplex, d($T_1A_2G_3T_4C_5A_6A_7$*$G_8G_9G_{10}C_{11}A_{12}$)−d($T_{13}G_{14}C_{15}C_{16}C_{17}T_{18}T_{19}G_{20}A_{21}C_{22}T_{23}A_{24}$), containing a 10*R* adduct at dA*$_7$ that corresponds to trans addition of the N^6-amino group of dA_7 to (−)-(*7S,8R,9R,10S*)-7,8-dihydroxy-9,10-epoxy-7,8,9,10-tetrahydrobenzo[*a*]pyrene [(−)-(*S,R,R,S*)-BP DE-2]. This DNA duplex contains the base sequence for the major dA mutational hot spot in the *HPRT* gene when Chinese hamster V79 cells are given low doses of the highly carcinogenic (+)-(*R,S,S,R*)-BP DE-2 enantiomer. NOE data indicate that the hydrocarbon is intercalated on the 5′-side of the modified base as has been seen previously for other oligonucleotides containing BP DE-2 (10*R*)-dA adducts. 2D chemical exchange-only experiments indicate dynamic behavior near the intercalation site especially at the 10*R* adducted dA, such that this base interconverts between the normal anti conformation and a less populated syn conformation. Ab initio molecular orbital chemical shift calculations of nucleotide and dinucleotide fragments in the syn and anti conformations support these conclusions. Although this DNA duplex containing a 10*R* dA adduct exhibits conformational flexibility as described, it is nevertheless more conformationally stable than the corresponding 10*S* adducted duplex corresponding to trans opening of the carcinogenic isomer (+)-(*R,S,S,R*)-BP DE-2, which was too dynamic to permit NMR structure determination. UV and imino proton NMR spectral observations indicated pronounced differences between these two diastereomeric 12-mer duplexes, consistent with conformational disorder at the adduct site and/or an equilibrium with a nonintercalated orientation of the hydrocarbon in the duplex containing the 10*S* adduct. The existence of conformational flexibility around adducts may be related to the occurrence of multiple mutagenic outcomes resulting from a single DE adduct.

Polycyclic aromatic hydrocarbons (PAH) are common environmental contaminants whose oxidative metabolism in mammals results in the formation of activated species that are cytotoxic, mutagenic, and/or carcinogenic. Benzo-ring diol epoxides in which the epoxide group is located in a bay region of the molecule have been implicated as ultimate carcinogens formed upon metabolism of carcinogenic PAHs (*1*). The prototypical PAH, benzo[*a*]pyrene (BP),[1] is metabolized to a diastereomeric pair of 7,8-diol 9,10-epoxides in which the benzylic hydroxyl group is either trans (DE-2) or cis (DE-1) to the epoxide oxygen. Furthermore, each of these diastereomers exists as a pair of enantiomers. For BP, only the major DE metabolite formed, (+)-(7*R*,8*S*,9*S*,10*R*)-7,8-dihydroxy-9,10-epoxy-7,8,9,10-tetrahydrobenzo[*a*]pyrene [(+)-(*R,S,S,R*)-BP DE-2], is tumorigenic in several animal models (*2*, *3*). The origin of these stereochemical differences is not currently understood.

The predominant adducts formed upon reaction of diol epoxides with DNA involve ring opening of the epoxide by cis or trans attack of the exocyclic N^2- and N^6- amino groups of guanine and adenine, respectively (*4*). At high doses of the tumorigenic (+)-(*R,S,S,R*)-BP DE-2 isomer, dG adducts account for the preponderance of mutations in the *HPRT* locus in Chinese hamster V79 cells. However, treatment of the cells with much lower doses such as might realistically result from metabolism of BP present in the environment results in a large increase in the relative proportion of mutations at dA (*5*, *6*). At very low doses (0.01−0.02 μM) of this BP DE, 25% of substitution mutations in the *HPRT* gene are A to C transversions (*6*). At these low doses of (+)-BP DE-2, the highest frequency of mutations was observed at the dA* ("hot spot") in the partial sequence 5′-dAGTCAA*GGGC-3′, where dA* corresponds to base 578 in the transcribed strand (*6*). Notably, no mutations were

† This research was supported by NIH (ES06839 and 1P30 ES06676), Welch Foundation (H-1296), and Sealy and Smith Foundation grants to D.G.G. Building funds were provided by the NIH (1CO6CA59098). The project was funded in part by an NIH fellowship to D.E.V. (T32 AI07536).

* Address correspondence to this author. Telephone: 409-747-6800; fax: 409-747-6850; e-mail: david@nmr.utmb.edu.

‡ University of Texas Medical Branch.

§ Present Address: MD Anderson Cancer Center, Houston, TX 77030-4095.

|| NIDDK.

[1] Abbreviations: rMD, restrained molecular dynamics; MORASS, multiple Overhauser relaxation analysis and simulation; BP, benzo[*a*]pyrene; DE, diol epoxide.

10.1021/bi001669l CCC: $19.00
Published on Web 10/25/2000

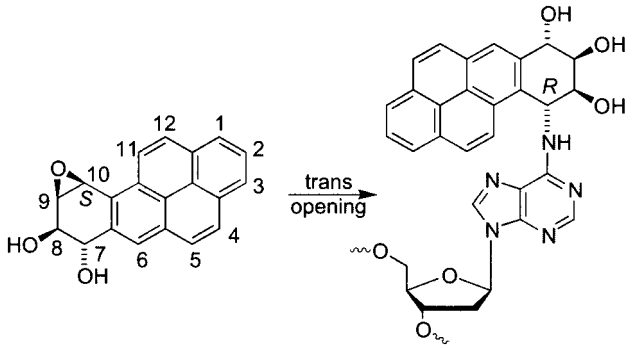

FIGURE 1: Trans addition of the exocyclic N^6 amino group of dA to (−)-(7*S*,8*R*,9*R*,10*S*)-7,8-dihydroxy-9,10-epoxy-7,8,9,10-tetrahydrobenzo[*a*]pyrene [(−)-(*S*,*R*,*R*,*S*)-BP DE-2]. Since the adducts arise by trans attack at C10, configuration of this carbon in the diol epoxide inverts upon adduct formation.

observed at the first dA in the dCAAG- sequence. The same dCAA- sequence also comprises codon 61 of the *N-ras* protooncogene, a triplet that is mutated upon activation to the oncogene in many tumors (*7*). Sequence context can have a profound influence on the type as well as the frequency of the mutations produced. Thus, Loechler and co-workers (*8*) have shown that a N^2 dG adduct derived from trans opening of (+)-(*R*,*S*,*S*,*R*)-BP DE-2 within a 5′-dCG*T sequence produces a G to A transition 82% of the time, whereas within a dTG*C sequence, a G to T transversion is found with 97% frequency. Loechler (*9*) hypothesized that the sequence dependence of mutational distributions is due to different types and/or distributions of major and minor conformations.

It has been recently demonstrated that mutational hot spots for BP DE may correlate with mutations associated with lung cancers. Mutations at a specific dG residue in the p53 gene in smokers' lung tumors correlate with hot spots for (+)-(*R*,*S*,*S*,*R*)-BP DE-2 adduct formation (*10*). This "smoking gun" strongly supports the importance of PAH and BP DE adducts in the etiology of human cancers.

Is there a unique feature of this sequence in the *HPRT* gene that makes it a hot spot for mutation? To help address this issue, we have investigated the structure of a duplex consisting of the oligomer 5′-d($T_1A_2G_3T_4C_5A_6A_7$*$G_8G_9G_{10}C_{11}A_{12}$)-3′ and its complementary strand 5′-d($T_{13}G_{14}C_{15}C_{16}C_{17}T_{18}T_{19}G_{20}A_{21}C_{22}T_{23}A_{24}$)-3′, which corresponds to this site. Two diastereomeric oligonucleotides were prepared, containing either a trans opened dA adduct of (+)-(*R*,*S*,*S*,*R*)-BP DE-2 [BP DE-2 (10*S*)-dA*$_7$ adduct] or of its noncarcinogenic enantiomer (−)-(*S*,*R*,*R*,*S*)-BP DE-2 [BP DE-2 (10*R*)-dA$_7$ adduct] at dA*$_7$ as indicated. Note that the configuration at C10 inverts upon trans opening of the epoxide; see Figure 1. In the present study, we describe the solution structure of the duplex containing the BP DE-2 (10*R*)-dA*$_7$ adduct derived from the (−)-(*S*,*R*,*R*,*S*)-BP DE-2 enantiomer. In contrast, the duplex containing the BP DE-2 (10*S*)-dA*$_7$ adduct derived from the carcinogenic (+)-(*R*,*S*,*S*,*R*)-BP DE-2 metabolite was intractable to detailed NMR structural studies, due to apparent motion near the adduct site, as shown by broad NMR signals. In addition, the lack of a UV red shift on duplex formation with this (10*S*)-dA*$_7$ adduct suggested that the stacking of the hydrocarbon with the adjacent DNA bases is weak.

MATERIALS AND METHODS

Preparation of Oligonucleotides. The adducted 12-mers, 5′-d($T_1A_2G_3T_4C_5A_6A_7$*$G_8G_9G_{10}C_{11}A_{12}$)-3′, containing trans opened (+)- and (−)-BP DE-2 adducts at A*$_7$ were prepared as a pair of diastereomers by solid-phase synthesis using the mixed diastereomers of N^6-[10β-(7β,8α,9α-triacetoxy-7,8,9,-10-tetrahydrobenzo[*a*]pyrenyl)]-5′-*O*-(4,4′-dimethoxytrityl)-3′-*O*-[(*N*,*N*-diisopropylamino)(β-cyanoethoxy)phosphynyl]-2′-deoxyadenosine (trans-BP DE-2 dA phosphoramidite) that had been synthesized from (±)-10β-amino-7β,8α,9α-trihydroxy-7,8,9,19-tetrahydrobenzo[*a*]pyrene (*11*) by the general method described (*12*). The oligonucleotide was constructed on 59 mg (7 μmol) of dA-controlled pore glass (cpg) (170 Å, 117 μmol/g) by automated synthesis (ABI model 392 synthesizer), with a manual step for coupling of the modified phosphoramidite [(20 μmol, ∼3-fold molar excess) with 100 μL of 0.5 M 1*H*-tetrazole in acetonitrile, ∼18−20 h]. End capping was omitted after the manual step to ensure that any adducted chains that had lost the 5′-dimethoxytrityl (DMT) group would be elongated in subsequent steps. Since, in our experience, recovery of the 5′-DMT substituted oligonucleotides on reverse phase HPLC was poor, and the two diastereomeric adducted oligonucleotides were not well-separated as their DMT derivatives, the terminal DMT protecting group was removed and the detritylated oligonucleotides were purified directly by HPLC on a Hamilton 7-μm PRP-1 column, 10 × 250 mm, eluted at 3 mL/min with a linear gradient that increased the composition of acetonitrile in 0.1 M $(NH_4)_2CO_3$ buffer, pH 7.5, from zero to 17.5% over 20 min. The two adducted 12-mers eluted at 18.0 and 18.7 min, whereas failure sequences lacking the hydrocarbon adduct elute much earlier (∼10−13 min). Typically, 30−60 A_{260} units of each pure, diastereomeric oligonucleotide were isolated from a 7-μmol synthesis. Circular dichroism (CD) spectra (see Supporting Information) of the early (10*R*) and late eluting (10*S*) oligonucleotides permitted assignment of their absolute configuration at the point of attachment of the purine to the hydrocarbon, on the basis of previous observations (*13*) that oligonucleotides containing 10*R* BP adducts at dA consistently exhibit positive CD bands for the pyrene chromophore in the 300−360 nm region, whereas their 10*S* diastereomers show negative bands in this region.

Thymidine-methyl-^{13}C (Cambridge Isotope Laboratories, Andover, MA) was converted to its 5′-DMT-3′-[(*N*,*N*-diisopropyl)-β-cyanoethyl]phosphoramidite (*14*) and purified by HPLC on an Axxiom silica column, 10 × 250 mm, eluted at 8 mL/min with CH_2Cl_2 containing 0.25% MeOH and 0.25% Et_3N (rt 2.8 min); *m*/*z* (FAB) 746 $(M+1)^+$. Synthesis of the isotopically labeled complementary strand, 5′-d$T_{13}G_{14}C_{15}C_{16}C_{17}$**[^{13}C]$T_{18}$**$T_{19}G_{20}A_{21}C_{22}T_{23}A_{24}$-3′, was carried out as described above on a 10-μmol scale using 128 μmol of the labeled phosphoramidite (12.8-fold molar excess) and 150 μL of 0.5 M 1*H*-tetrazole in acetonitrile in the manual coupling step. After cleavage of base labile protecting groups (58 °C, overnight), the oligonucleotide was purified as its 5′-DMT derivative by HPLC on the Hamilton PRP-1 column, eluted at 3.5 mL/min with a linear gradient that increased the acetonitrile concentration in the aqueous $(NH_4)_2CO_3$ buffer from 22.5 to 28.5% over 12 min; T_r 10.8 min. After removal of the DMT group (80% HOAc in H_2O, 30 min, rt)

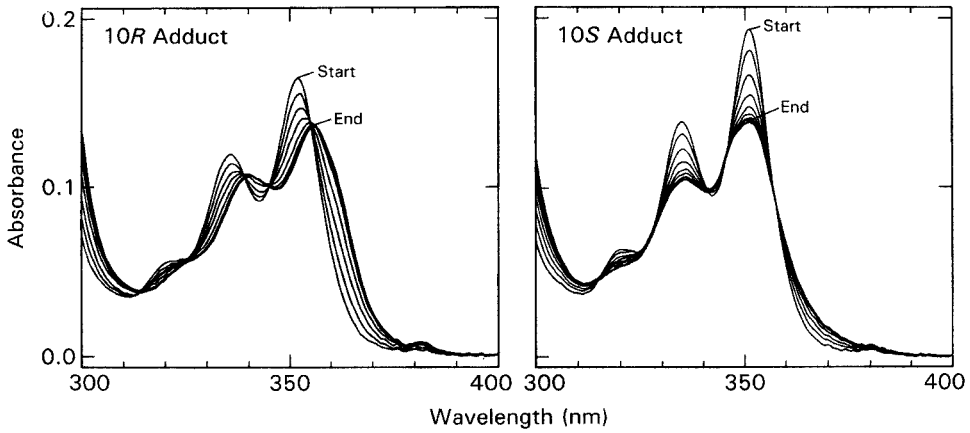

FIGURE 2: UV spectrophotometric titration of the 10*R*- (left panel) and 10*S*- (right panel) adducted 12-mers (~0.9 A_{260}/mL) with their complementary strand at 25 °C in the phosphate-NaCl buffer described in the text. The spectrum marked Start corresponds to the adducted strand in the absence of any complement; the spectrum marked End corresponds to the end point of the titration (stoichiometric formation of duplex) where further additions of the complementary strand produce no additional spectral change.

the oligonucleotide was chromatographed on the Hamilton PRP-1 column eluted at 3.5 mL/min with the solvent gradient described above for the detritylated, adducted oligonucleotides; T_r 15.1 min.

Sample Preparation. To determine the correct stoichiometry for formation of the 1:1 duplex, each adducted oligonucleotide containing a BP DE-2 10*R* or 10*S* adduct at dA_7 was titrated with its complementary strand, 5′-$dT_{13}G_{14}C_{15}C_{16}C_{17}T_{18}T_{19}G_{20}A_{21}C_{22}T_{23}A_{24}$-3′, at 25 °C by measuring the absorbance decrease at 353 nm on duplex formation in an aqueous buffer containing 12 mM Na_2HPO_4, 8 mM NaH_2PO_4, and 56 mM NaCl (total ionic strength 100 mM) as described (*15*) (Figure 2). At this temperature, the end point, at which no absorbance change occurred on further addition of the complement, corresponded to a ratio of 1.0 A_{260} unit of complement/1.2 A_{260} units of adducted strand. The ratio determined from UV titration of a small sample of each oligonucleotide was then used in the preparation of NMR quantities of the duplexes. Melting temperatures of the modified and unmodified duplexes (~10 μM total strand concentration) were determined in the same buffer by UV spectroscopy at 270 nm as described (*12*). For NMR studies, these adducted duplexes were dissolved in 0.5 mL of the above phosphate-NaCl buffer (final pH 6.7) containing 50 μM sodium azide.

NMR Experiments. All proton experiments were carried out on Varian UNITYplus 750 and 600 and/or Varian VXR500S spectrometers. One-dimensional spectra for nonlabile (aromatic and aliphatic) and labile (imino and amino) protons were obtained using WET1D and BINOM pulse sequences, respectively. NOESY experiments were carried out using the WETNOESY pulse sequence (*16*). NOESY experiments carried out in 99.96% D_2O were done at 15 °C at 750.258 MHz with 4096 complex points in t_2 and 512 complex points in t_1, sweep widths of 7455.7 Hz and a relaxation delay of 4.3 s. The 200 ms mixing time NOESY carried out in 90% H_2O/10% D_2O was done at 5 °C at 599.800 MHz with 8192 complex points in t_2 and 512 complex points in t_1, sweep widths of 12001 Hz, and a relaxation delay of 3.8 s. 90° shifted sine-bells were applied to both dimensions of the NOESY experiments before Fourier transformation. Z-filtered TOCSY (*17*) experiments were recorded with 50 and 120 ms mixing times. ROESY (*18*, *19*) and exchange-only experiments (*20*) were recorded with 200 and 150 ms mixing times, respectively. A DQF-COSY (*21*) experiment was recorded at 15 °C. The data were processed using VNMR on SUN Sparc 10 and Sparc 20 workstations or Silicon Graphics Inc. (SGI) workstations.

Restrained Molecular Dynamics Calculations. The NMR structure refinement followed a MORASS/AMBER protocol that has been previously described (*15*). Calculations were performed on a SGI Indigo2 workstation. 453 nonexchangeable proton distance restraints were derived from our hybrid relaxation matrix program, MORASS 2.5 (*22*), using NOE volumes from a 200-ms NOESY done in 99.96% D_2O. Sixty exchangeable proton NOE restraints were produced by assigning strong (1.75−3.50 Å), medium (1.75−4.25 Å), and weak (1.75−5.50 Å) intensities to cross-peaks from a 90% H_2O/10% D_2O NOESY at 600 MHz. A total of 522 NOESY flat well constraints [453 nonexchangeable, 60 exchangeable, and 9 imino proton restraints (all base pairs except for dA_7−T_{18} and the base pairs on either side)] were used for refinement during our 5 ps AMBER 5 (*23*) molecular dynamics simulations at 300 K for the final round. Earlier rounds used only the 453 nonexchangeable and 9 imino proton restraints. The coordinates of the last picosecond of MD were averaged using CARNAL (*24*), and this average coordinate set was refined by 2000 steps of full conjugate gradient minimization with NOESY restraints. The starting structure for these calculations was standard B form DNA that contained a normal anti glycosidic angle at the adducted deoxyadenosine. AMBER solvated sodium counterions were included in all structure calculations.

The progress of the iterative refinement process was monitored by several key factors, indicating the match between experimental NOESY volumes and theoretical NOESY volumes calculated from the refined structure. The RMS errors in the volumes were used as the first criterion for monitoring the refinements (*25*). The % RMS (volume) is given by

$$\%\ \text{RMS (volume)} = \sqrt{1/N \sum_{ij} \left(\frac{v_{ij}^a - v_{ij}^b}{v_{ij}^a} \right)^2} \times 100\%$$

where *a* or *b* can be either the experimental or theoretical

2D volumes to give the % RMS (exp) or % RMS (the), respectively.

The *R*-factor that is similar to the *R*-factor used in X-ray crystallography was also used as a refinement criterion (*26*). The *R*-factor is given by

$$R = \frac{\sum_{ij} |v_{ij}^a - v_{ij}^b|}{\sum_{ij} v_{ij}^a}$$

where *a* represents experimental volumes and *b* represents theoretical volumes.

We have suggested that the % RMS (volume) is a very useful measure of quality of fit to the spectra since it weighs the percentage differences in the theoretical and experimental volumes for both large and small cross-peaks equally. The *R*-factor is regarded as a poorer measure of the quality of the refined structure since it is often dominated by the largest cross-peaks. Another quality of fit, the $Q^{1/6}$ factor (*26*), also better reflects the quality of the structure since it weighs more heavily on the weak cross-peaks (longer, interresidue distances) as compared to the *R*-factor. The $Q^{1/6}$ factor used in MORASS is defined as

$$Q(1/6) = \frac{\sum_{ij} \tau_m |(v_{ij}^a)^{1/6} - (v_{ij}^b)^{1/6}|}{\sum_{ij} (1/2)\tau_m |(v_{ij}^a)^{1/6} + (v_{ij}^b)^{1/6}|}$$

where *a* represents theoretical volumes and *b* represents experimental volumes.

A 70-ps unrestrained molecular dynamics calculation was undertaken using the structure from round 5 of the MORASS/rMD/minimization cycles as the starting structure, and the 50 lowest energy structures from the last 50 ps were minimized. The 50 structures were grouped into 10 clusters using the CalcCluster module in MolMol (*27*) with a maximum RMSD of 1 Å within each cluster. An average structure was determined for each of these clusters [CARNAL (*24*)], and these averaged structures were refined by 2000 steps of full conjugate gradient minimization with NOESY restraints to yield the final 10 structures. The coordinates of these 10 final structures were then averaged (CARNAL) and subsequently minimized with NOESY restraints to provide the final average structure. All structures were built with XLEAP (*28*) and displayed with MolMol or MIDAS2.1 (*29*).

Ab Initio Calculations of the Chemical Shifts of A_6 and A_7 Including the Hydrocarbon. As discussed below, the chemical exchange spectrum provides evidence for conformational changes surrounding the adducted dA site. These changes could result from either a change in sugar pucker at dA_6 between C2′-endo and C3′-endo (*30*) and/or rotation of the χ glycosidic torsional angle to the adducted adenine (*31*). Ab initio SCF molecular orbital calculations [Gaussian 94 (*32*)] at the RHF/6-31G* level of theory were carried out (SGI Octane R10K) to determine the effect of (i) a change in sugar pucker at dA_6 and (ii) syn-anti interconversion of dA^*_7 on the theoretical chemical shifts for the H8 and H2 protons of dA^*_7 and H2 of dA_6 in the $d(pA_6pA^*_7)$ dinucleotide segment of our present structure. In one set of calculations, the dA_6 sugar was fixed in either the C2′-endo conformation or the C3′-endo conformation. In a second set, the glycosidic torsional angle, χ, of the adducted dA in this dinucleotide was constrained in either an anti or syn conformation. As a control, ab initio calculations were also carried out on the major (syn) and minor (anti) conformers of the adducted $d(pA_5)$ mononucleotide in a 9-mer duplex containing a BP DE-2 (10*S*)-dA adduct with a dG mismatch. As a result of slow interconversion between the two conformations of this mismatched duplex, we had previously been able to assign chemical shifts for the major and minor conformers, corresponding to syn and anti glycosidic torsions, respectively, of the adducted dA (*31*, *33*).

In each case, the coordinates for the ab initio calculation were obtained by taking either the di- or mononucleotide directly from the final MORASS calculated structure of the oligonucleotide in question. A 5′-phosphate was retained with each structure. The 5′-phosphate and the 3′-hydroxyl oxygen were then each terminated with a methyl group using GaussView (*32*). The two terminal methyl groups were subsequently minimized in GaussView while keeping the rest of the molecule fixed. The resulting structures provided the input coordinates to Gaussian94. Each calculation required ca. 5 days of CPU time. All proton chemical shifts were calculated by comparison with water protons calculated at the same level of theory.

RESULTS AND DISCUSSION

Nonexchangeable Proton NMR Spectra and Chemical Shift Assignments. The labeling convention for the hydrocarbon and absolute configuration for the BP DE-2 (10*R*)-dA adduct are shown in Figure 1. The DNA proton chemical shift assignments were made utilizing NOESY, TOCSY, ROESY, and DQF-COSY experiments and by following established methods for canonical DNA (*34*). Figure 3 shows the base to H1′ region of the 2D NOESY spectrum. The sequential connectivity is shown by solid lines for the adducted strand in Figure 3, panel A, and for the complementary strand in Figure 3, panel B. Although connectivities are drawn for illustration from the dA_6 H8 and dC_5 H6 base protons to the dC_5 H1′ proton, NOESY peaks are not observed for these correlations. A NOESY peak from dC_5 H6 to T_4 H1′ is observed however. In general, sequential connectivities were missing or very broad from residue dA_6 to both dC_5 and dA^*_7. No cross-peaks were observed from the H8 proton of dA_6 to the deoxyribose protons of dC_5, and cross-peaks between dA^*_7 H8 and the deoxyribose protons of dA_6 were broad and weaker than expected. Typical cross-peaks were observed for the remaining bases of this strand and all bases in the complementary strand.

To facilitate identification of the two adjacent thymidine residues in the complementary strand, T_{18} with a ^{13}C label in the methyl group was incorporated into this strand in the position opposite the adducted dA^*_7. The protons of this methyl group could thus be unambiguously identified by their ^{13}C splitting. These protons (0.44 ppm) as well as H6 (6.08 ppm) are shifted by about 1 ppm upfield from typical values, indicating that they are stacked above or below the aromatic portion of the BP DE-2, consistent with intercalation of the hydrocarbon into the helix. Additional evidence for intercalation is the weak inter H1′ to base proton NOE between dA_6 and dA_7 (Figure 3). The intra H1′ to H6 NOE for dC_5 is missing as well as the inter H1′ to H8 NOE between dC_5 and dA_6. The dC_5 residue protons were assigned using

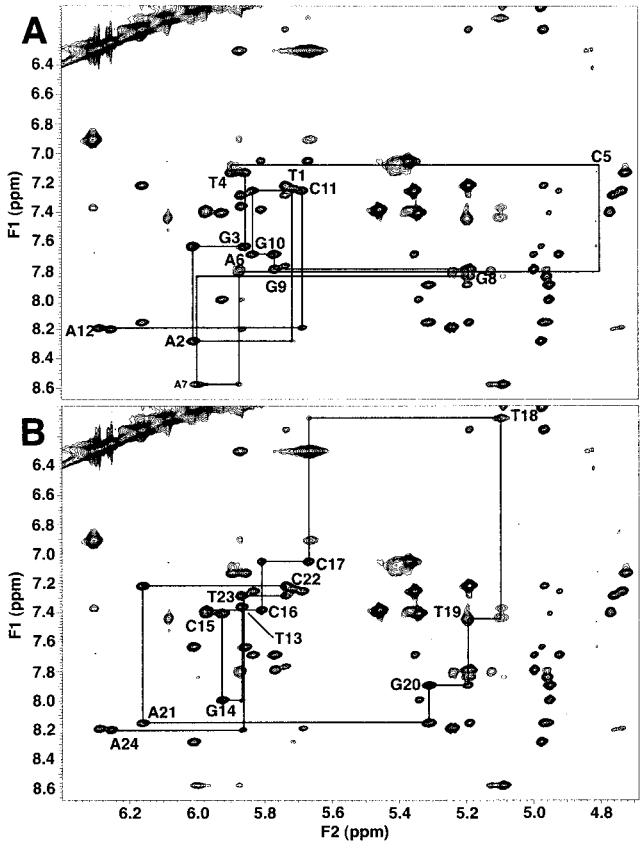

FIGURE 3: The base (F1) and H1′ (F2) proton region of a 200-ms mixing time NOESY experiment of the 12-mer duplex in D_2O. (A) The sequential connectivity (solid lines) between the base and the H1′ protons of the adducted strand, d($T_1A_2G_3T_4C_5A_6A^*_7G_8G_9G_{10}C_{11}A_{12}$), where the A^*_7 represents the BP DE-2 (10*R*)-dA adduct and (B) the sequential connectivity of the complementary strand, d($T_{13}G_{14}C_{15}C_{16}C_{17}T_{18}T_{19}G_{20}A_{21}C_{22}T_{23}A_{24}$). Note the unusually upfield shifted T_{18} H6 position (6.08 ppm).

TOCSY and DQF-COSY data. The difficulty in assigning almost all of the dC_5 protons is due to their broad line widths, which are indicative of dynamic motion involving dC_5. The chemical shift assignments for the DNA and hydrocarbon protons are listed in Tables 1 and 2, respectively.

Benzo[*a*]*pyrene Protons*. The protons of the BP DE-2 system were assigned using both TOCSY (Figure 4, panels A and B) and NOESY (Figure 4, panel C) data, as well as comparisons to other BP DE systems (*30*, *33*). Aromatic protons H11 and H12 were readily assigned by their relatively upfield chemical shifts, 6.30 and 6.91 ppm, respectively, and confirmed in both the TOCSY (Figure 4, panel B) and NOESY (Figure 4, panel C) data. An NOE peak (Figure 4, panel C) and a weak TOCSY peak (Figure 4, panel A) between H11 and H10 (5.66 ppm) provided a connection between the aromatic and the aliphatic portions of the BP DE-2. The remaining aliphatic BP DE-2 protons were assigned by sequential TOCSY peaks (Figure 4, panel A) and by NOESY peaks (data not shown). In Figure 4, panel A, the H9−H8 cross-peak on one side of the diagonal is missing due to water saturation, so the connectivities of H9 to both H10 and H8 are indicated with a single line. The H1 proton was assigned based on a strong NOE peak from H12 to a resonance at 7.37 ppm. A strong TOCSY peak from H1 to 7.43 ppm was used to assign H2. Aliphatic proton H7 on the other side of the BP DE-2 had a strong NOE to a proton at 8.19 ppm, which was assigned to H6. A strong NOE between H6 and a signal at 7.82 ppm was attributed to an interaction between H5 and H6. A resonance at 7.53 ppm was assigned to H4 based on both TOCSY and NOE peaks from 7.53 to 7.82 ppm (H5). Finally, an NOE peak from H4 to a resonance at 7.44 ppm was attributed to an H3−H4 interaction. Definitive cross-peaks between H2 and H3 could not be observed because of their nearly degenerate chemical shifts, 7.43 and 7.44 ppm, respectively.

Evidence for 5′ Direction of Intercalation for the Hydrocarbon from DNA to BP NOEs. The BP H10, H11, and H12 protons are located on the edge of the hydrocarbon that is nearest to the modified deoxyadenosine, dA^*_7. There are several NOEs from protons on dA_6, the nucleotide 5′ to dA^*_7, and the BP H10, H11, and H12 protons. BP H10 has NOEs to dA_6 H1′, H2′, H2″, H3′, and H8. BP H11 has NOEs to dA_6 H1′, H2′, H2″, and H8. BP H12 has an NOE to dA_6 H1′. These NOEs are evidence that the edge of the hydrocarbon near the site of adduction is pointed toward dA_6 in the 5′ direction relative to dA^*_7.

The BP H1, H2, H3, H4, H5, and H6 protons are located on the edge of the hydrocarbon farthest away from dA^*_7. There are NOEs from T_{18}, the base complementary to dA^*_7, to this far edge of the BP. BP H1 has NOEs to T_{18} H6 and

Table 1: Chemical Shift Assignments (in ppm) of the DNA Protons

residue	H1′	H2′	H2″	H3′	H4′	H6/8	H2/5/Me	NH(2)[a]
dT_1	5.71	1.62	2.10	4.56	3.93	7.24	1.51	
dA_2	6.00	2.82	2.89	4.97	4.35	8.29		
dG_3	5.85	2.45	2.65	4.82	4.36	7.64		12.66
dT_4	5.89	1.81	2.18	4.72	4.09	7.14	1.16	13.62
dC_5	4.80	1.30	1.34	4.51	3.81	7.09	5.40	8.28, 6.82
dA_6	5.87	2.99	2.81	5.13	4.31	7.81	6.74	
dA_6[b]							7.40[b]	
dA^*_7	5.99	2.83	2.87	5.09	4.43	8.58	7.69	6.67
dA^*_7[b]						7.37[b]	8.62[b]	
dG_8	5.19	2.58	2.66	4.95	4.25	7.84		12.90
dG_9	5.76	2.63	2.73	4.99	4.36	7.80		13.02
dG_{10}	5.83	2.46	2.63	4.92	4.31	7.69		12.98
dC_{11}	5.68	1.88	2.24	4.73	4.05	7.26	5.35	8.35, 6.64
dA_{12}	6.28	2.61	2.40	4.64	4.14	8.19		
dT_{13}	5.86	1.86	2.27	4.62	4.36	7.36	1.57	
dG_{14}	5.92	2.73	2.73	4.95	4.36	8.00		12.88
dC_{15}	5.97	2.19	2.44	4.77	4.23	7.41	5.34	8.22, 6.49
dC_{16}	5.80	1.87	2.25	4.66	4.00	7.38	5.46	8.32, 6.81
dC_{17}	5.66	1.21	1.60	4.44	3.80	7.06	5.37	8.38, 7.02
dT_{18}	5.10	1.72	1.99	4.59	3.85	6.08	0.44	11.63
dT_{19}	5.19	2.13	2.25	4.60	3.93	7.45	1.95	12.82/11.88
dG_{20}	5.31	2.71	2.71	4.95	4.30	7.90		12.57
dA_{21}	6.16	2.68	2.81	4.96	4.40	8.16	7.77	
dC_{22}	5.73	1.81	2.29	4.60	4.24	7.22	5.19	8.06, 6.75
dT_{23}	5.86	1.97	2.28	4.76	4.02	7.29	1.58	
dA_{24}	6.25	2.63	2.40	4.65	4.13	8.20		

[a] Imino and amino protons. [b] Minor conformer.

Table 2: BP DE-2 Proton Chemical Shifts[a]

proton	δ (ppm)	proton	δ (ppm)
H1	7.37	H7	5.24
H2	7.43	H8	3.98
H3	7.44	H9	4.83
H4	7.53	H10	5.66
H5	7.82	H11	6.30
H6	8.19	H12	6.91

[a] Corresponding chemical shifts for the BP DE-2 protons in the N-ras 11-mer (30) were within 0.0−0.05 ppm of those observed in the present study.

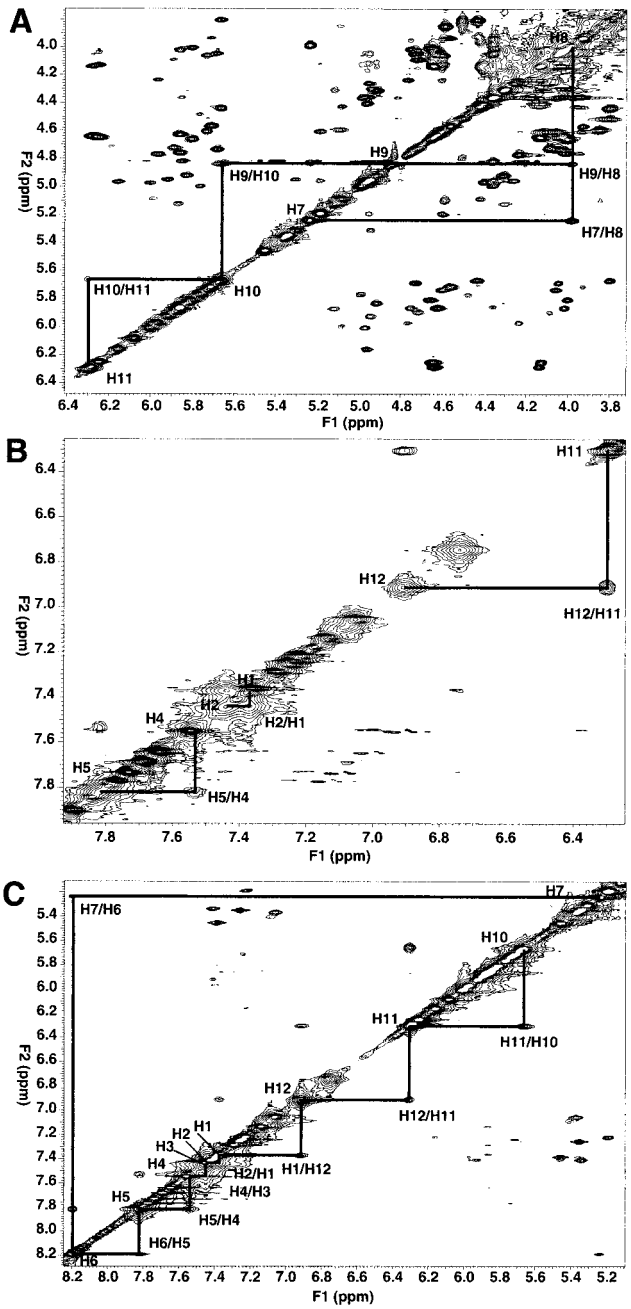

FIGURE 4: (A) 120 ms mixing time TOCSY spectrum of the aliphatic proton region of the BP DE moiety (H7, H8, H9, H10). (B) The aromatic proton region of the above TOCSY spectrum containing protons H1, H2, H3, H4, H5, H6, H11, and H12. The spin system H1−H2−H3 gives a single cross-peak due to the degeneracy of H2 and H3. (C) 150 ms mixing time NOESY spectrum of the aromatic pyrene proton region.

H1′. In addition, T_{18} H6 has NOEs to BP H2, H3, and H4. The methyl protons of T_{18} have NOEs to BP H3, H4, H5, and H6. These NOEs from the BP moiety to T_{18} are indicative of hydrocarbon intercalation.

Exchangeable DNA Proton Spectra. All of the exchangeable base protons for the present adducted 12-mer could be assigned by a 2D NOESY spectrum taken in 90% H_2O buffer solution, except for the terminal base pairs at each end of the duplex. Both imino to imino (Figure 5, panel A) and imino to H2 (Figure 5, panel B) proton NOE peaks were used to assign the exchangeable protons, which are listed in Table 1. As shown in Figure 5, the spectrum clearly establishes Watson−Crick base pairing between the modified dA^*_7 and the T_{18} opposite on the unmodified strand by the presence of a weak NOE from the imino proton of T_{18} to the H2 proton of dA^*_7. The base-to-base connectivity in the imino water/NOESY spectrum shows a break between base pairs $dA^*_7-T_{18}$ and dA_6-T_{19} which is presumably due to intercalation of the hydrocarbon between them (Figure 5, panel A). Further, the large upfield chemical shift of the dA_6-T_{19} imino proton is associated with the location of these bases on the 5′-side of the pyrene ring system. A larger upfield shift is observed for the $dA^*_7-T_{18}$ imino proton. In addition to the NOE between the T_{19} and G_{20} imino protons, the T_{19} imino proton has a weak NOE to a resonance at 11.88 ppm that appears to be a minor conformation of T_{19} possibly associated with a change in glycosidic torsion angle of base dA^*_7 and subsequent repositioning of the BP DE ring system (see below).

Structure Refinement of the Major Conformer. Although it was clear from peak broadening in the vicinity of the adduct as well as the presence of several chemical exchange cross-peaks (see below) that dynamic behavior involving one or more minor conformations was occurring, it was possible to refine a structure for the major conformer. Because of fast chemical exchange for the vast majority of the peaks and a small population for the minor conformer, the single set of observed NOE cross-peaks measured is largely associated with the major conformer or an averaged structure representing both major and minor conformations. However, some of the calculated distances may be in error because of the presence of a finite population of the minor form. Several different starting model structures for the major conformer were considered. All NOEs were consistent with a B-DNA duplex, and this was used as an initial model. The NOESY spectra provided unambiguous evidence that in the major form of the adduct, the dA^*_7 base was in the anti glycosidic conformation, and the water/NOESY spectrum showed that it was base paired to T_{18}. The observed NOEs indicated that the hydrocarbon was intercalated, rather than in the major or minor groove, consistent with all previous NMR structures for BP DE dA adducts (*15*, *30*, *31*, *33*, *35*−*37*) including the same trans opened BP DE-2(10*R*)-dA adduct in a related *N-ras* sequence (*30*). NOEs also established that the BP ring was intercalated on the 5′-side of the adducted base as observed in all other BP DE (10*R*)-dA adducts (*15*, *30*, *35*−*37*).

The progress of the iterative MORASS/rMD structural refinement starting from a B-DNA model with the hydrocarbon intercalated from the major groove is shown in Table 3. All of the volumes merged by the fifth iteration of the MORASS/rMD structural refinement, and the final total restraint energy penalty in round 5 was 231.8 kcal/mol. In the final iterations, 522 distance restraints were incorporated into the refinement with 17 of them between the nonexchangeable hydrocarbon protons and the DNA duplex. The measure of the quality of the refinement ($Q^{1/6}$) decreased to 0.0778 in the final MORASS iteration. The structure from this round was subjected to 70 ps of free MD and the 50 lowest energy structures in the last 50 ps were used to generate 10 structures (see experimental details) from which an average structure was determined. MORASS was used to determine the quality of all 10 structures as well as for the average structure. The final (averaged) structure has a

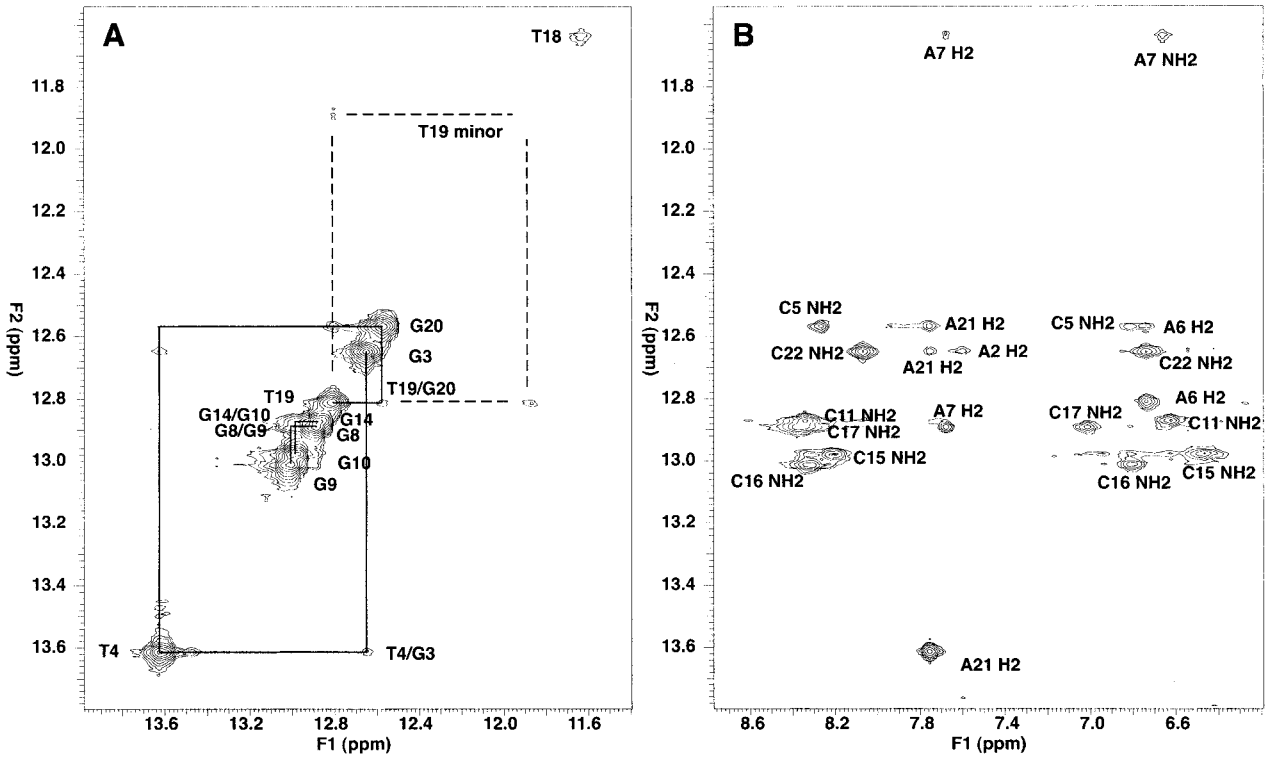

FIGURE 5: Expanded regions of a 150-ms mixing time H_2O NOESY spectrum of the 12-mer duplex showing NOE peaks from the imino protons to (A) imino protons or (B) H2 and amino protons. Base pair-to-base pair connectivity can be traced from G_3 to T_4, T_4 to G_{20} (base paired with C_5), and G_{20} to T_{19}, and from G_8 to G_9 and G_{10} to G_{14} (base paired to C_{11}). The G_9 and G_{10} imino protons are nearly degenerate. The broadened imino proton of T_{18} (which is base paired to the BP DE-2-adducted A_7) does not have an NOE to either the T_{19} or G_8 imino protons, although T_{19} does have an NOE to a resonance at 11.88 ppm which has no diagonal peak. This resonance may correspond to a minor conformation of the T_{19} imino proton.

Table 3: MORASS Structure Calculation Progression

iteration[a]	% RMS[b]$_{vol}$	*R*-factor	$Q^{1/6}$ factor	$E_{(amber)}$	$E_{(Const)}$	force[c]/% error
0	10594.2	0.6074	0.1184			
1	310.84	0.5927	0.0997	−1582.9	53.2	10/25
2	145.41	0.5881	0.1025	−1577.6	66.1	5/20
3	104.95	0.5947	0.0876	−1482.3	430.1	5/13
4	131.62	0.5451	0.0851	−1460.6	382.8	15/11
5	85.57	0.5412	0.0778	−1473.8	231.8	17(10)[d]/10
6 (SA)[e]	91.9	0.4938	0.0745	−1450.2	250.6	20(10)[d]/10
⟨SA⟩ [f]	84.0 ± 9.5	0.4775 ± 0.022	0.0737 ± 0.0013	−1427.1 ± 20.7	311.2 ± 32.2	20(10)[d]/10

[a] MORASS iteration number. [b] The average of the % RMS differences between the experimental and theoretical volumes. [c] Flatwell potential function parameters (force constant in kcal/mol Å^2; error is the permitted error on the constraining distances). [d] The number in parentheses is the force constant applied to 60 additional restraints derived by estimating NOE strengths from data in H_2O involving exchangeable protons. [e] Values for the final average structure (SA). [f] ⟨*SA*⟩ Average values for the 10 cluster derived structures.

$Q^{1/6}$ factor of 0.0745, an *R*-factor of 0.4938, and a % RMS$_{vol}$ of 91.9% (Table 4). The average values of the structure quality factors for the 10 structures are $Q^{1/6} = 0.0737 \pm 0.0013$, $R = 0.4775 \pm 0.022$, and % RMS$_{vol} = 84.0 \pm 9.5$. The quality factors for the final average structure are higher than the averages of the factors for the 10 structures. This reflects the fact that 3 of the 10 structures fit significantly worse than the remaining seven and that the number of structures within each cluster were not used to weight the averaging for the final structure. The RMSD of the NOE deviations for the average structure is 0.086 ± 0.147 Å; however, the number of NOE violations greater than 0.3 and 0.5 Å, 50 and 16, respectively, is relatively large. In a similar structure, Stone and co-workers (*30*) reported 24 ± 4 deviations greater than 0.3 Å. The RMS deviations of bond lengths and angles of the final 10 structures from ideal geometry are 0.0118 ± 0.0002 Å and 2.878 ± 0.062°, respectively. The pairwise RMSD for the heavy atoms of the starting B-DNA model structure and the final average structure is 3.36 Å, while the average RMSD of the 10 final structures as compared to the final averaged structure is 1.14 ± 0.27 Å for the central 10 base pairs. The RMSD of the heavy atoms near the adducted site (residues 6, 7, 18, and 19) is 1.22 ± 0.25 Å.

In the final structure, the hydrocarbon remains intercalated in the 5′ direction from the modified dA*$_7$, and T_{18} is stacked underneath the aromatic portion of the hydrocarbon (Figure 6). To accommodate the bulky lesion, both the T_{18}-dA*$_7$ and T_{19}-dA_6 base pairs are buckled away from the intercalated BP DE-2. Although no hydrogen bond restraints were used for these base pairs in the structure refinements, the hydrogen bonds of both base pairs remain intact. The T_{19} O4 oxygen is only 1.75 Å from the closest dA_6 amino proton, and the T_{19} H3 proton is 2.16 Å from the dA_6 nitrogen N1. The

Table 4: Analysis of the MORASS/MD Generated Structures of the BP DE-2 10*R* Adduct

NMR Distance Constraints	
total no. of distance restraints	522
interresidue restraints	179
intraresidue restraints	314
BP DE restraints	17
H-bonding restraints (empirical)	9
Structural Statistics	
NMR $Q^{1/6}$ factor	
final averaged structure	0.075
best-fitting structure	0.072
worst-fitting structure	0.077
rmsd of NOE violations (Å)	0.086 ± 0.147
NOE violations > 0.5 Å	16
NOE violations > 0.3 Å	50
RMS deviations from ideal geometry	
bond length (Å)	0.0118 ± 0.0002
bond angle (°)	2.878 ± 0.062
pairwise rmsd (Å) over heavy atoms	
final ave vs starting model	3.36
final ave vs 10 clusters	1.14 ± 0.27
worst cluster vs cluster	2.81
best cluster vs cluster	1.80

corresponding distances for the T_{18}−dA*$_7$ base pair are 2.02 and 2.31 Å, respectively. The structure is further stabilized by three hydrogen bonds between the BP DE-2 hydroxyl protons (purple) and the DNA. The O4 oxygen of T_{18} (royal blue) is only 1.60 Å from the BP DE-2 hydroxyl group proton at carbon C7, and the O2P nonbridging oxygen of dA_6 is 1.44 Å from the hydroxyl proton at C9 of BP DE and 1.60 Å from the hydroxyl proton at C8 of BP DE. The deoxyribose rings of both dA_6 and dA*$_7$ are in a C2′-endo conformation.

Several other refinements were carried out in which the dA_6 sugar ring was constrained to either the C2′-endo or C3′-endo conformations. The $Q^{1/6}$ value for the dA_6 C2′-endo constrained structure was 0.0815 and for the dA_6 C3′-endo constrained structure was 0.0831. These differences are too small to distinguish whether the dA_6 sugar ring was C2′-endo or C3′-endo. Therefore, no sugar pucker constraints were used in the structures reported. In all three structures (sugar unconstrained, C2′-endo or C3′-endo constrained), the final refined structure of the major form (Figure 6) shows the hydrocarbon intercalated from the major groove, between the dA*$_7$-dT_{18} and the dA_6-T_{19} base pairs with an overall B-DNA duplex geometry. The modified dA*$_7$ remained in the anti conformation, forming a normal Watson−Crick base pair to the opposite T in all three NMR structure calculations.

Chemical Exchange-Only Spectra: Evidence for a Minor Conformer. Three relatively large cross-peaks observed in the base region of the 100 ms NOESY spectra could not be assigned to any of the typical interactions observed in NOESY experiments and were thus presumed to be chemical exchange peaks for the dA*$_7$ H2 (7.68 and 8.62 ppm), dA*$_7$ H8 (8.58 and 7.36 ppm), and dA_6 H2 (6.74 and 7.40 ppm) protons (Figure 7, panel A). That these peaks arise from a chemical exchange process was verified by a 150-ms chemical exchange-only experiment (Figure 7, panel B) in which NOESY and ROESY peaks are eliminated. In the chemical exchange-only experiment, three significant peaks are detected on both sides of the diagonal. These correspond to the three unassigned peaks indicated in the NOESY experiment. Therefore, both the dA_6 and the dA*$_7$ bases appear to be involved in some chemical exchange dynamics that dramatically alters the environments of the dA_6 H2 and dA*$_7$ H8 and H2 protons.

After the D_2O sample had been kept at room temperature for 45 days, most of the labile H8 base protons had exchanged with the solvent deuterium atoms, and a second 100-ms NOESY spectrum was acquired (Figure 7, panel C). In this subsequent 100-ms NOESY experiment, the cross-peak assigned to the dA*$_7$ H8 proton is no longer observed. However, the cross-peaks for the H2 protons of dA*$_7$ (7.69 and 8.62 ppm) and dA_6 (6.74 and 7.40 ppm) are still observed. These observations validate the assignments of these three peaks despite the rather large downfield chemical shift observed for the H2 proton of dA*$_7$ in the minor conformation (8.62 ppm). In all three spectra, the cross-peak for the dA_6 H2 proton is significantly stronger and broader than the other cross-peaks, suggesting that the dynamics at this residue may be different from that of residue dA*$_7$ (perhaps involving a conformational inversion of the sugar ring). The absence of several sequential NOESY peaks from both dA*$_7$ and dC_5 to the dA_6 residue is presumably due to this dynamic behavior. Because of peak overlap in the spectrum of the unexchanged sample, it was not possible to quantify the population of the minor conformation. However, after deuterium exchange of the labile H8 protons, the intensity of the overlapping protons was reduced enough (Figure 7, panel C) that we could estimate from signal integration that the population of the minor conformer was less than 5% (major conformer > 95%).

Weak NOESY peaks between the dA*$_7$ H8 proton in the minor form and resonances at 6.08, 5.66, and 5.19 ppm were also observed (data not shown). The resonance at 6.08 may be the minor form of the dA*$_7$ H1′ proton, which has a chemical shift of 5.99 ppm in the major form. Although the chemical shift of the T_{18} H6 proton is 6.08 ppm, an NOE interaction between the T_{18} H6 and dA*$_7$ H8 protons is highly unlikely given the long distance between them. A strong NOE should be observed between the H8 and H1′ protons in a nucleoside with a syn conformation, although the signal intensity would be a function of the syn population. Thus, the weak intensity of the cross-peak between the minor form of the dA*$_7$ H8 proton and the resonance at 6.08 ppm is consistent with a small population of dA*$_7$ in the syn form. The resonance at 5.19 ppm may be the minor form of the dA*$_7$ H3′ proton which has a chemical shift of 5.09 ppm in the major form, and the resonance at 5.66 may correspond to the BPDE H10 proton. Additional weak NOE peaks are observed. Although we may speculate on the origins of these data, they cannot be unambiguously assigned given their weak intensities and small number.

We considered two possibilities for the conformational interchange with a minor species that gives rise to the chemical exchange cross-peaks. These are (i) interconversion between a C2′-endo and C3′-endo conformation of the sugar of dA_6, as previously reported by Stone and colleagues for a related *N-ras* sequence (dCAA*G) in an 11-mer duplex containing the same BP DE-2 (10*R*)-dA adduct (*30*) and (ii) interconversion between syn and anti conformations of the adducted dA*$_7$, as demonstrated by us for two conformations that are resolvable on the NMR time scale for a BP DE-2 (10*S*)-dA adduct in a 9-mer duplex with a mismatched dG opposite the adduct (*31*, *33*). Our NMR data for the present

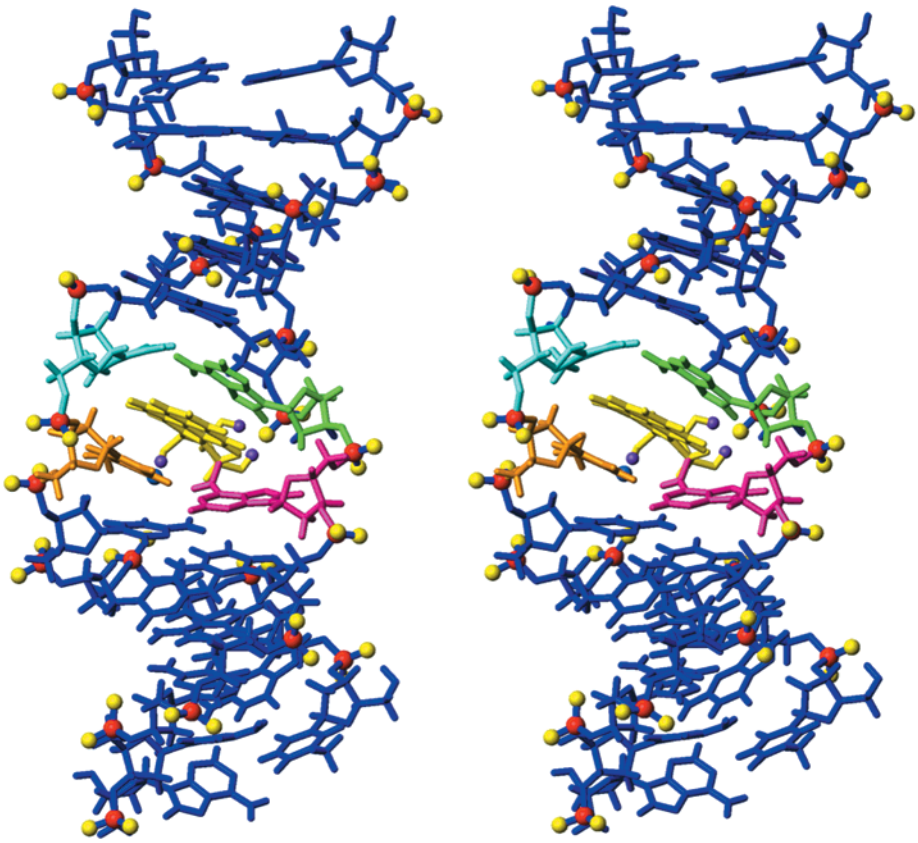

FIGURE 6: Stereoview of the refined structure of the major conformer (anti conformation at $dA*_7$) of the 12-mer duplex containing a trans opened DE-2 (10*R*)-dA adduct. The deoxyribose ring and base of the adducted $dA*_7$ are shown in pink and the BP DE-2 system is shown in yellow. Bases T_{18}, T_{19}, and dA_6 are orange, cyan, and green, respectively. Phosphate groups are shown with red phosphorus atoms and yellow nonbridging oxygen atoms (O1P and O2P). The O4 oxygen (royal blue) of T_{18} forms a hydrogen bond (1.60 Å) with the BP DE-2 hydroxyl proton (purple) at carbon C7, and the O2P oxygen of dA_6 forms hydrogen bonds with the BP DE-2 hydroxyl protons (purple) at carbons C8 and C9.

12-mer are insufficient to distinguish between these two possibilities. In the present duplex, the population of the minor conformer is much smaller (on the order of 5%) than in the mismatched 9-mer (83% syn/17% anti), making identification of weak cross-peaks extremely difficult, even at 750 MHz. Furthermore, the rate of chemical exchange for the present duplex is faster on the NMR time scale than that for our previous mismatched 9-mer, so that only those protons (H2 and H8) that have a large chemical shift difference in the two conformations are observed separately, whereas other protons give very broad or averaged signals. The two protons with large chemical shift differences between the major and minor conformations, dA_7 H8 ($\Delta\delta = 1.21$ ppm) and dA_7 H2 ($\Delta\delta = 0.93$ ppm), exhibit relatively narrow peaks in the exchange-only spectrum. In contrast, the dA_6 H2 proton, which has a smaller chemical shift difference between the two conformations ($\Delta\delta = 0.66$) provides an extremely broad exchange-only peak. In the BP DE-2 (10*S*)-dA adduct in a 9-mer duplex with a mismatched dG opposite the adduct (*31*, *33*) the chemical shift differences for the BPDE protons in the two conformations were all less than 0.5 ppm and all but three were less than 0.15 ppm. Thus, while the BPDE moiety and dC5 are undoubtedly involved in the conformational exchange process, the small magnitude of the chemical shift changes precludes the observation of related exchange-only cross-peaks and provides broad averaged signals in the NOESY data.

Ab Initio Calculations of the Chemical Shifts of dA_6 and $dA*_7$ Including the Hydrocarbon. To help differentiate between these two competing explanations, we carried out ab initio molecular orbital chemical shift calculations at the RHF/6-31G* level of theory for the protons and heavy atoms of the $d(pA_6pA*_7)$ dinucleotide of our present duplex. In a pair of calculations using the geometry from our refined structure with the anti conformation of $dA*_7$, the dA_6 sugar was constrained to either the C2′-endo or the C3′-endo conformation. The corresponding chemical shift calculations with $dA*_7$ in the C2′-endo, syn conformation were also carried out. Since we have no experimentally derived structure for the syn conformation in the present 12-mer, we accomplished the necessary χ torsional rotation by driving it with a series of highly restrained AMBER minimizations. We used the $d(pA*_5)$ mononucleotide from the major (syn) and minor (anti) conformers of the (10*S*) dA adduct in our previously studied mismatched 9-mer (*31*, *33*) as a model to see if the ab initio calculations can accurately predict the switch in chemical shifts observed for H8 and H2 of the adducted dA when the glycosidic angle, χ, rotates between syn and anti.

Can the change in sugar pucker at dA_6 alone account for the differences seen in the chemical shifts of the chemical exchange peaks for H8 and H2 of dA_7 and H2 of dA_6? The ab initio calculations of the chemical shifts of the $d(pA_6pA*_7)$ dinucleotide containing the hydrocarbon suggest that the chemical exchange peaks seen for H2 of dA_6 and H2

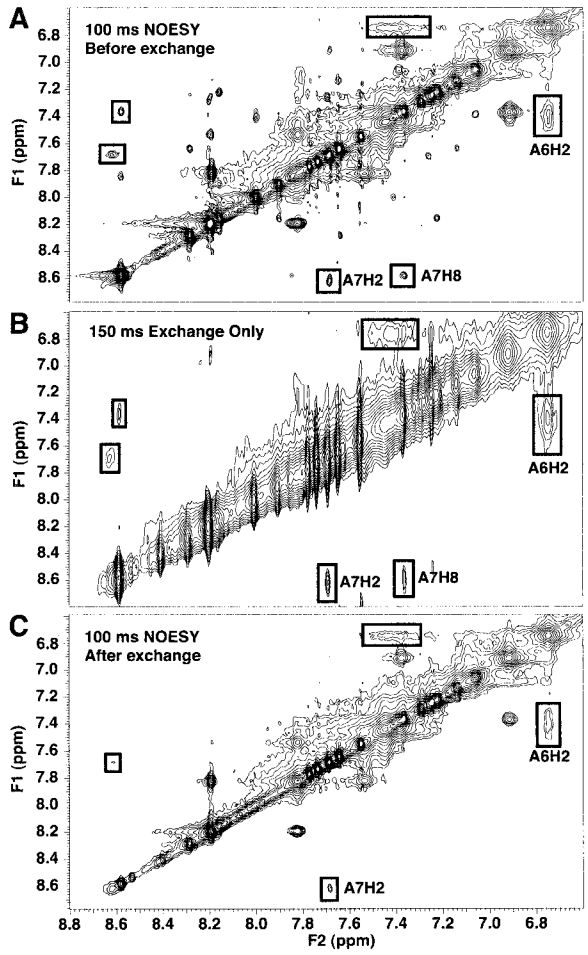

FIGURE 7: Base proton region of three spectra collected on the 12-mer duplex: (A) a 100 ms mixing time NOESY spectrum in 99.96% D_2O, (B) a 150 ms mixing time chemical exchange-only experiment in D_2O, and (C) a 100 ms mixing time NOESY spectrum in 99.6% D_2O in which most of the H8 protons (ca. 80%) have been exchanged with solvent deuterium atoms. Cross-peaks due to chemical exchange processes are noted for H8 and H2 of the adducted residue ($dA*_7$) and for H2 of dA_6.

and H8 of dA_7 are not due solely to a change of the dA_6 sugar pucker from C2′-endo to C3′-endo. The calculated chemical shift values for the H2 protons of $dA*_7$ and dA_6 with the dA_6 sugar pucker fixed in either C2′-endo or C3′-endo are similar (Table 5) and do not predict the substantial differences in chemical shift seen in the exchange-only data. Thus the chemical shift of the dA_6 H2 proton signal is calculated to change only from 7.69 to 7.68 ppm if the sugar flips from a C2′-endo to C3′-endo conformation. Similarly, the $dA*_7$ H2 proton shifts only 0.05 ppm upon this conformational change.

In contrast, the ab initio calculations predict large differences in chemical shifts for H8 and H2 of an adducted dA upon syn−anti interconversion. Most importantly, they accurately predict the direction of the chemical shift changes observed for the H8 and H2 protons of a BP DE-2 (10*S*)-dA adduct in the mismatched 9-mer whose major (syn) and minor (anti) solution conformers have been assigned by 2D NMR (*31*, *33*) (Table 5). The calculations correctly predict a ca. 1 ppm downfield shift for this H8 proton when the dA* converts from a syn to an anti conformation, in contrast to the upfield shift of nearly the same magnitude predicted and observed for the H2 proton. In all but one case (H8 of $dA*_5$ syn), the values of the calculated and observed chemical shifts agree within ± 0.2 ppm. Interestingly, the large chemical shift differences between the syn and anti conformers do not appear to result primarily from interactions with a neighboring or complementary base, since the calculations for the isolated $d(pA*_5)$ of the 9-mer correctly predict these differences.

Similar chemical shifts observed for the present 12-mer duplex are fully in accord with the hypothesis of a rotation of the $dA*_7$ base from anti to syn in the minor conformer (Table 5). The observed chemical shift for H2 of $dA*_7$ is 7.69 in the major conformation. The calculated chemical shift for this proton in the anti conformation is 7.74 ppm (for a C2′-endo dA_6 sugar conformation), consistent with the assigned anti conformation (based on NOE data, see above) of the major species. From the chemical exchange spectra, the corresponding H2 chemical shift in the minor (putative syn) conformation is 8.62 ppm. We anticipate that the chemical shift for the H2 proton of the adducted dA in a syn conformation should shift ~1 ppm to lower field upon anti to syn rotation [experimental value for the 9-mer, 7.93 ppm (anti) to 8.72 (syn)], in good agreement with the experimental downfield shift from 7.69 (major) to 8.62 ppm (minor) for the present 12-mer. Similarly, the observed and calculated chemical shifts for H8 of $dA*_7$ in the major (anti) conformer of the 12-mer are 8.58 and 8.88 ppm (for a C2′-endo dA_6 sugar conformation), respectively. We anticipate that the chemical shift for H8 of the adducted dA in a syn conformation should shift to ~1 ppm higher field [8.73 ppm (anti) to 7.81 (syn) for the 9-mer], consistent with our experimental upfield shift from 8.58 (major) to 7.37 ppm (minor) for this proton in the 12-mer. As shown in Figure 6, depending upon the glycosidic conformation for the adducted dA, either the H2 or H8 protons will be stacked under the aromatic ring of the BP DE, producing large ring current shifts, as reflected in these calculations.

Despite excellent agreement between the experimental and calculated chemical shifts for $dA*_7$, the experimental and calculated chemical shifts for dA_6 are significantly different for the major conformation. The experimental chemical shifts for the H2 and H8 protons of dA_6 are 0.95 and 0.75 ppm upfield from those predicted by theory for the major conformation ($dA*_7$ anti) in which dA_6 is restricted to the C2′-endo conformation. In contrast, the experimental (7.40 ppm) and calculated (7.37 ppm) chemical shifts for the dA_6 H2 proton in the minor conformation agree quite well. In addition, the chemical shift of the dA_6 H8 proton (7.81 ppm) agrees quite well with the calculated chemical shift for the major conformation ($dA*_7$ anti) in which the dA_6 deoxyribose is in the C3′-endo conformation (7.75 ppm), suggesting that residue dA_6 may be undergoing a C2′-endo to C3′-endo conversion as previously noted by Stone and co-workers (*30*). The poor agreement between theory and experiment for the dA_6 H2 and H8 protons in the major, anti conformation may be a reflection of the poor quality of the structure at this position. No NOE peaks were observed from the dA_6 H8 proton to the dC_5 deoxyribose protons, and those observed from dA_6 to either $dA*_7$ or the hydrocarbon were weak and very broad. Because the dA_6 base is stacked above the BP DE system, a small change in their relative positions could result in significant shielding differences.

Table 5: Comparison of Experimentally Determined Proton Chemical Shifts with ab Initio Calculated Chemical Shifts for Key Protons with Detectable Chemical Exchange Cross Peaks

proton (conformation at adducted dA*)	calculated[a], ppm C2′-endo	calculated[a], ppm C3′endo	experimental (ppm)[b]	exchange peaks[c]
A_6H2 (A*$_7$ *anti*)	7.69	7.68	6.74[d]	yes
A_6H2 (A*$_7$ *syn*)	7.37		7.40[e]	
A_6H8 (A*$_7$ *anti*)	8.56	7.75	7.81[d]	no
A_6H8 (A*$_7$ *syn*)	8.43			
A*$_7$H2 (A*$_7$ *anti*)/A*$_5$H2 (A*$_5$ *anti*)[f]	7.74/7.67[f]	7.69	7.69[d]/7.93[f]	yes
A*$_7$H2 (A*$_7$ *syn*)/A*$_5$H2 (A*$_5$ *syn*)[f]	8.16/8.65[f]		8.62[e]/8.72 [f]	
A*$_7$H8 (A*$_7$ *anti*)/A*$_5$H8 (A*$_5$ *anti*)[f]	8.88/8.50[f]	9.36	8.58[d]/8.73 [f]	yes
A*$_7$H8 (A*$_7$ *syn*)/A*$_5$H8 (A*$_5$ *syn*)[f]	7.07/6.88[f]		7.37[e]/7.81 [f]	

[a] Chemical shifts are derived from ab initio calculations. See Methods for details. [b] Chemical shifts for 12-mer derived from this study from a 200-ms mixing time NOESY experiment. [c] Chemical shifts derived from a 150-ms mixing time chemical exchange-only experiment. See Methods for details. [d] Chemical shift of the 12-mer major conformation. [e] Chemical shift of the 12-mer minor conformation. [f] Chemical shifts (A*5) for the 9-mer; experimental values are from Schwartz et al. (*33*). Syn and anti glycosidic angles at nucleotide dA5* correspond to the major and minor solution conformations, respectively. Chemical exchange cross-peaks are seen at the positions of the major and minor dA5* H2 and H8 chemical shift values.

Table 6: Comparison of Chemical Shifts of the *HPRT* 12-mer (present study) and *N-ras* 11-mer (30) Duplexes[a]

base	H1′	H2′	H2″	H3′	H4′	H6/8	CH_3/H5
			adducted strand				
C_5	4.80 (4.44)	1.30 (0.92)	1.34 (1.22)	4.51 (4.01)	3.81 (3.94)	7.08 (6.78)	5.40 (4.96)
A_6	5.87 (5.81)	2.99 (2.63)	2.81 (2.92)	5.13 (5.08)	4.31 (4.25)	7.81 (7.67)	
A_7	5.99 (5.88)	2.83 (2.75)	2.87 (2.82)	5.09 (5.05)	4.43 (4.38)	8.58 (8.56)	
G_8	5.19 (4.93)	2.58 (2.53)	2.66 (2.63)	4.95 (4.21)	4.25 (4.06)	7.84 (7.84)	
			complementary strand				
C_{17} (C_{15})	5.66 (5.68)	1.21 (1.31)	1.60 (1.62)	4.44 (4.48)	3.80 (3.98)	7.06 (7.08)	5.37 (5.38)
T_{18} (T_{16})	5.10 (5.10)	1.72 (1.73)	1.99 (1.98)	4.59 (4.60)	3.85 (4.25)	6.08 (6.09)	0.44 (0.46)
T_{19} (T_{17})	5.19 (5.31)	2.13 (2.20)	2.25 (2.36)	4.60 (4.63)	3.93 (4.18)	7.45 (7.45)	1.95 (1.95)
G_{20} (G_{18})	5.31 (5.90)	2.71 (2.68)	2.71 (2.77)	4.95 (4.92)	4.30 (4.35)	7.90 (7.94)	

[a] Values not in parentheses are for the present *HPRT* 12-mer duplex; values in parentheses are the chemical shifts for the corresponding protons in the N-ras 11-mer (*30*).

The above calculations and comparisons support our conclusion that the observed exchange peaks result from interconversion of the adducted dA*$_7$ between an anti and a syn orientation in these two conformers, respectively, and they clearly indicate that the large chemical shift differences for H2 and H8 of dA*$_7$ between the two conformers do not result from changes in the sugar pucker of dA_6 alone. Indeed, the calculations are consistent with either a C2′-endo or C3′-endo conformation (or a combination of these) since the predicted chemical shift differences resulting from this conformational change are generally small. Thus it is quite possible that, in addition to the syn/anti interconversion of dA*$_7$, such a C2′-endo/C3′-endo interconversion also takes place with the present oligonucleotide but is not experimentally detected because of the time scale on which it is occurring. As far as we are aware, ab initio calculations of chemical shift at this high level of theory have not been reported for a system this large in applications to biomolecular structures.

It is possible that syn−anti interconversion of the glycosidic torsion angle takes place in addition to the dA_6 sugar pucker interconversion in the 11-mer containing a sequence surrounding the *N-ras* codon 61 (*30*). However, one should be cautious when interpreting the results of these two related structural studies, because the sequence context outside the central four base pairs is different. Indeed as shown in Table 6, while the chemical shifts of the dA_6A_7*G_8 sequence within the $dC_5A_6A_7$*G_8 sequence of both the N-*ras* and *HPRT* sequences are quite similar, the chemical shifts of the dC_5 (and its complementary base) are quite different, suggesting some degree of conformational variation (at least on the 5′-side of the adduct) between the *ras* and *HPRT* sequences.

Comparison of Diastereomeric BP DE-2 (10R)- and (10S)-dA Adducts: Possible Roles of Adduct Conformation and Sequence in Dynamics of Adducted Duplexes. Our synthetic approach yields the diastereomeric, adducted oligonucleotides corresponding to trans opening of the two enantiomers of (±)-BP DE-2 by the exocyclic amino group of dA_7. Since these diastereomeric oligonucleotides are generally quite conveniently separated by reverse phase HPLC, a single synthetic procedure generates both structures. Absolute configurations of the separated diastereomers at C10, the point of attachment of the base to the hydrocarbon, were assigned on the basis of their CD spectra as described in the Materials and Methods (cf. Supporting Information).

A goal of the present study was to compare the solution structure of the 12-mer duplex that contains the trans opened (10*S*)-dA adduct derived from the carcinogenic and metabolically most significant (+)-(*R*,*S*,*S*,*R*)-BP DE-2 isomer with the oligonucleotide containing the corresponding 10*R* adduct, whose precursor diol epoxide lacks significant tumorigenic activity. UV spectral observations indicated pronounced differences between these two diastereomeric 12-mer duplexes and suggested that the duplex containing the (10*S*)-dA adduct is conformationally disordered at the adduct site and/or exists in part in conformation(s) in which the hydrocarbon is not intercalated into the DNA: (i) Upon titration (Figure 2) of the 10*R* adducted oligonucleotide that is the subject of this NMR study with its T-containing complementary strand, a red shift of the pyrene bands occurs

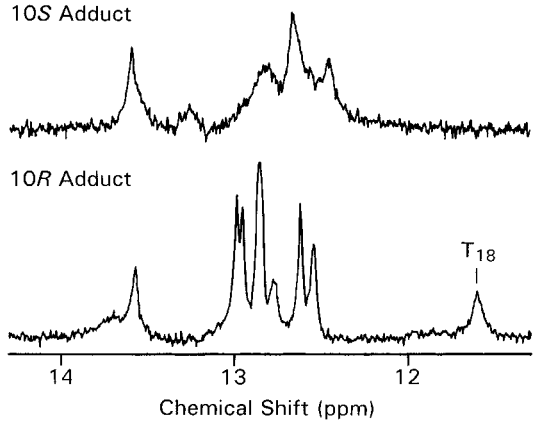

FIGURE 8: NMR spectra at 500 MHz (H_2O, 5 °C) for the imino proton region of the 12-mer duplex containing the trans opened BP DE-2 (10*S*) adduct at dA*$_7$ (upper trace), and of the same duplex containing the diastereomeric trans opened BP DE-2 (10*R*) adduct that is the subject of this NMR study (lower trace). For the 10*S* adducted duplex, note the broad signals and the lack of any observable signals in the 9−12 ppm region characteristic of base paired imino protons adjacent to the adduct.

as the duplex is formed, diagnostic of intercalation of the aromatic hydrocarbon into the duplex (left panel) and consistent with our NMR structure. In contrast, the diastereomeric, 10*S* adducted duplex (right panel) shows no red shift relative to the single strand. (ii) T_m values in the phosphate/NaCl buffer used for the NMR studies were 47 and 37 °C for the duplexes containing the present (10*R*)-dA adduct and its 10*S* diastereomer, respectively, as compared with 50 °C for the normal duplex. Lower T_m values are generally typical of oligonucleotides containing 10*S* as opposed to 10*R* BP adducts at dA (*38*). (iii) The UV spectra in the pyrene region for the present, 10*R* adducted 12-mer duplex, measured as a function of temperature, are consistent with normal melting behavior between 30 and 65 °C (shift of λ_{max} to shorter wavelength and increase in absorbance due to loss of stacking) and are essentially independent of temperature below 30 °C. In contrast, spectra of the diastereomeric 10*S* adducted duplex are temperature-dependent well below the T_m, such that λ_{max} shifts to shorter wavelength by approximately 3−4 nm, and the absorbance increases slightly on cooling from 30 to 7 °C (*38*). Both the blue shift and the absorbance increase suggest a conformational change of the duplex on cooling that favors conformation(s) in which the hydrocarbon is not intercalated.

Further evidence for conformational heterogeneity of the 10*S* adducted duplex was obtained from the imino proton spectrum in water (Figure 8). Even at 5 °C, the imino proton signals are weak, broad, and poorly resolved, suggestive of weak base pairing in this duplex. Most significantly, the absence of any detectable signals between 9 and 12 ppm, the region in which base paired imino protons directly above or below the modified dA*$_7$ normally appear, suggests high conformational flexibility near the adduct site. An attempt to slow the dynamics of the duplex structure by use of 20 mM imidazole buffer, pH 7, containing 100 mM $MgCl_2$ (which increased the intensity of the blue shifted band at low temperature and raised the T_m by 11 °C under UV spectrophotometric conditions) resulted in an even poorer appearance of its imino proton spectrum (*38*). Apparent conformational disorder at the adduct site in the 10*S* adducted 12-mer thus precluded attempts to determine its solution structure by NMR.

In all intercalated dA DE adducts studied to date, the absolute configuration at the point of attachment determines to which side of the modified dA residue the hydrocarbon will intercalate, such that the aromatic portion is intercalated to the 3′-side of the modified adenine for adducts with *S* configuration at the site of attachment to the base at this carbon and to the 5′-side for adducts with *R* configuration. When the parent hydrocarbon is BP, oligonucleotide duplexes containing 10*S* adducts with a normal T complement have thus far been too disordered to permit determination of their solution conformations by NMR (*38*). However, NMR structures have been determined for duplexes with complementary T opposite both (1*R*)- and (1*S*)-dA adducts derived from benzo[*c*]phenanthrene (BPh) DE-2 (*39*, *40*) and benzo[*a*]anthracene (BA) DE-2 (*41*, *42*). Interestingly, 1*S* adducts from both these hydrocarbons show evidence for minor conformers, whereas minor conformers were not detected for their 1*R* diastereomers. Thus, ∼20% of a minor conformer with a syn glycosidic torsional angle was observed for an oligonucleotide duplex containing a BA DE-2 (1*S*)-dA adduct at the first A in the partial sequence dCA*AG (*42*). Notably, the syn conformer is actually the major one for a BP DE-2 (10*S*)-dA adduct when it is stabilized by base pairing with a dG mismatch (*31*, *33*).

We previously proposed (*35*) that part of the difference in stability between (10*R*)- and (10*S*)-dA adducts of BP DEs arises from steric interference between the DNA and the aliphatic portion of the DE that is more severe with the 10*S* than the 10*R* adducts, because of a tilting of the hydrocarbon (whose aromatic portion is intercalated at the 3′-side of the modified base) that places the partially saturated ring close to the DNA bases on the more hindered, 5′-side. Changing the glycosidic torsion angle from anti to syn moves the aliphatic portion of the hydrocarbon out and away from the 5′-base pair and thus relieves some of the unfavorable steric interactions, as indicated in the solution structure of the BP DE-2 (10*S*)-dA adduct with a dG mismatch (*31*, *33*). This analysis suggests that chirality at the point of attachment of the hydrocarbon to the adenine base contributes to the preference for a syn (*S*) vs anti (*R*) glycosidic torsion angle of the adducted dA when the aromatic portion of the hydrocarbon is intercalated.

Interestingly, even with the 10*R* adducted duplex that is the subject of the present NMR study, there is evidence for significant conformational dynamics near the lesion site. These results as well as those of Stone and co-workers (*30*) for the *N-ras* sequence discussed above suggest that in at least some cases oligonucleotide duplexes containing a trans opened BP DE-2 (10*R*)-dA adduct may also show dynamic behavior. Since the contributions of minor (10*R*)-dA adduct conformers to the NMR in both these cases are subtle, and may have been present but not detected in previous studies using different sequences, the role of sequence in promoting such dynamic behavior is at present a fascinating, but open, question. Our observations constitute the first clear evidence for a minor conformer of a 10*R* adduct in which the modified base is in the unusual syn conformation. In the present 10*R* adduct, however, the contribution of this conformational motif is small in comparison with the contributions of syn conformers in duplexes containing *S* adducts (*31*, *42*).

Although the equilibrium for the present adduct lies quite far toward the anti conformer, the energy difference between the two conformers is less than 2 kcal/mol, and perturbations in the environment, such as binding to an enzyme, could easily shift the equilibrium position.

The *S* dA-adducts in oligonucleotides are formed upon trans ring opening of the tumorigenic (*R*,*S*,*S*,*R*)-DE-2 stereoisomers, whereas the corresponding *R* adducts are derived from trans opening of their (*S*,*R*,*R*,*S*)-DE-2 enantiomers, which are generally only weakly tumorigenic or nontumorigenic. In a related study of dG adducts (presumably groove bound) using ligase-induced circularization experiments, Geacintov and co-workers (*43*) demonstrated that duplexes containing such trans opened (10*S*)-dG adducts derived from the tumorigenic (+)-(*R*,*S*,*S*,*R*)-BP DE-2 are also more flexible and bent than either the unmodified duplexes or the duplexes containing the corresponding (10*R*)-dG adducts derived from the weakly or nontumorigenic enantiomer, (−)-(*S*,*R*,*R*,*S*)-BP DE-2. A correlation has been proposed (*9*) between the distribution of mutations and conformational heterogeneity of the modified DNA. In the case of the dA adducts, an important factor contributing to such conformational heterogeneity is equilibration between the syn and anti conformations of the torsion angle between the adducted base and its sugar, as documented in this and other (*31*, *33*, *42*) NMR studies.

SUPPORTING INFORMATION AVAILABLE

Circular dichroism spectra of the purified, single-stranded oligonucleotide 12-mers containing the (10*R*)- and (10*S*)-BP DE-2 adducts at dA*$_7$ (1 page). This material is available free of charge via the Internet at http://pubs.acs.org. Coordinates have been deposited, PDB ID 1FYY.

REFERENCES

1. Thakker, D. R., Yagi, H., Levin, W., Wood, A. W., Conney, A. H., and Jerina, D. M., (1985) in *Bioactivation of Foreign Compounds* (Anders, M. W., Ed.) pp 177−242, New York Academic Press, New York.
2. Buening, M. K., Wislocki, P. G., Levin, W., Yagi, H., Thakker, D. R., Akagi, H., Koreeda, M., Jerina, D. M., and Conney, A. H. (1978) *Proc. Natl. Acad. Sci. U.S.A. 75*, 5358−5361.
3. Slaga, T. J., Bracken, W. J., Gleason, G., Levin, W., Yagi, H., Jerina, D. M., and Conney, A. H. (1979) *Cancer Res. 39*, 67−71.
4. Jerina, D. M., Chadha, A., Cheh, A. M., Schurdak, M. E., Wood, A. W., and Sayer, J. M. (1991) *Covalent Bonding of Bay-Region Diol Epoxides to Nucleic Acids.* In *Biological Reactive Intermediates IV. Molecular and Cellular Effects and Their Impact on Human Health.* (Witmer, C. M., Snyder, R., Jollow, D. J., Kalf, G. F., Kocsis, J. J., and Sipes, I. G., Eds.) pp 533−553, Plenum Press, New York.
5. Wei, S.-J. C., Chang, R. L., Wong,.C.-Q., Bhachech, N., Cui, X. X., Hennig, E., Yagi, H., Sayer, J. M., Jerina, D. M., Preston, B. D., and Conney, A. H. (1991) *Proc. Natl. Acad. Sci. U.S.A., 88*, 11227−11230.
6. Wei, S.-J. C., Chang, R. L., Bhachech, N., Cui, X. X., Merkler, K. A., Wong,.C.-Q., Hennig, E., Yagi, H., Sayer, J. M., Jerina, D. M., and Conney, A. H. (1993) *Cancer. Res. 53*, 3294−3301.
7. Barbacid, M. (1987) *Annu. Rev. Biochem. 56*, 779−827.
8. Shukla, R., Liu, T. M., Geacintov, N. E., and Loechler, E. L. (1997) *Biochemistry 36*, 10256−10261.
9. Loechler, E. L. (1995) *Mol. Carcinog. 13*, 213−219.
10. Denissenko, M. F., Pao, A., Tang, M. S., and Pfeifer, G. P. (1996) *Science 274*, 430−432.
11. Lakshman, M. K., Sayer, J. M., and Jerina, D. M. (1991) *J. Am. Chem. Soc. 113*, 6589−6594.
12. Lakshman, M. K., Sayer, J. M., Yagi, H., and Jerina, D. M. (1992) *J. Org. Chem. 57*, 4585−4590.
13. Christner, D. F., Lakshman, M. K., Sayer, J. M., Jerina, D. M., and Dipple, A. (1994) *Biochemistry 33*, 14297−14305.
14. Beaucage, S. L. (1993) *Methods Mol. Biol. 20*, 33−61.
15. Schurter, E. J., Yeh, H. J. C., Sayer, J., Lakshman, M. K., Yagi, H., Jerina, D. M., and Gorenstein, D. G. (1995) *Biochemistry 34*, 1364−1375.
16. Smallcombe, S. H., Patt, S. L., Keifer, P. A. (1995) *J. Magn. Reson. 117*, 295−303.
17. Rance, M. (1987) *J. Magn. Reson. 74*, 557−564.
18. Bothner-By, A., Stephens, R. L., and Lee, J.-M. (1984) *J. Am. Chem. Soc. 106*, 811−813.
19. Bax, A., and Davis, D. G. (1985) *J. Magn. Reson. 63*, 207−213.
20. Macura, S., Westler, W. M., and Markley, J. L. (1994) *Two-Dimensional Exchange Spectroscopy of Proteins*; in *Methods in Enzymology*; Vol. 239, pp 106−144, Academic Press, San Diego.
21. Piantini, U., Sorenson, O. W., and Ernst, R. R. (1982) *J. Am. Chem. Soc. 104*, 6800−6801.
22. Meadows, R., Post, C. B., Luxon, B. A., and Gorenstein, D. G. (1996) *MORASS* Program, University of Texas Medical Branch, Galveston, TX.
23. Case, D. A., Pearlman, D. A., Caldwell, J. W., Cheatham, T. E. I., Ross, W. S., Simmerling, C. L., Darden, T. A., Merz, K. M., Stanton, R. V., Cheng, A. L., Vincent, J. J., Crowley, M., Ferguson, D. M., Radmer, R. J., Seibel, G. L., Singh, U. C., Weiner, P. K., Kollman, P. A. (1997) *AMBER 5*, University of California, San Francisco.
24. Ross, W. S. (1994) *CARNAL*, University of California, San Francisco.
25. Post, C. B., Meadows, R., and Gorenstein, D. G. (1990) *J. Am. Chem. Soc. 112*, 6796.
26. James, T. L. (1991) *Curr. Opin. Struct. Biol. 1*, 1042−1053.
27. Koradi, R., Billeter, M., and Wuthrich, K. (1996) *MOLMOL: A Program for Display and Analysis of Macromolecular Structure*, Institute for Molecular Biology and Biophysics, Swiss Federal Institute of Technology, Zürich, Switzerland.
28. Schafmeister, C. E. A. F., Ross, W. S., and Romanovski, V. (1995) *LEaP*. University of California, San Francisco.
29. Ferrin, T. E., Huang, C. C., Jarvis, L. C., and Langridge, R. (1988) *J. Mol. Graphics 6*, 13−27.
30. Zegar, I. S., Chary, P., Jabil, R. J., Tamura, P. J., Johansen, T. N., Lloyd, R. S., Harris, C. M., Harris, T. M., and Stone, M. P. (1998) *Biochemistry 37*, 16515−16528.
31. Yeh, H. J. C., Sayer, J. M., Liu, X.-H., Altieri, M. S., Byrd, R. A., Lakshman, M. K., Yagi, H., Schurter, E. J., Gorenstein, D. G., and Jerina, D. M. (1995) *Biochemistry 34*, 13570−13581.
32. Frisch, M. J., Trucks, G. W., Schlegel, H. B., Gill, P. M. W., Johnson, B. G., Robb, M. A., Cheeseman, J. R., Keith, T., Petersson, G. A., Montgomery, J. A., Raghavachari, K., Al-Laham, M. A., Zakrzewski, V. G., Ortiz, J. V., Foresman, J. B., Cioslowski, J., Stefanov, B. B., Nanayakkara, A., Challacombe, M., Peng, C. Y., Ayala, P. Y., Chen, W., Wong, M. W., Andres, J. L., Replogle, E. S., Gomperts, R., Martin, R. L., Fox, D. J., Binkley, J. S., Defrees, D. J., Baker, J., Stweart, J. P., Head-Gordon, M., Gonzales, C., and Pople, J. A. (1995) *Gaussian 94*. Gaussian, Inc. Pittsburgh, PA.
33. Schwartz, J. L., Rice, J. S., Luxon, B. A., Sayer, J. M., Xie, G., Yeh, H. J. C., Liu, X., Jerina, D. M., and Gorenstein, D. G. (1997) *Biochemistry 36*, 11069−11076.
34. Wuthrich, K. (1986) *NMR of Proteins and Nucleic Acids*; John Wiley and Sons: New York.
35. Schurter, E. J., Sayer, J. M., Oh-hara, T., Yeh, H. J. C., Yagi, H., Luxon, B. A., Jerina, D. M., and Gorenstein, D. G. (1995) *Biochemistry 34*, 9009−9020.
36. Jerina, D. M., Sayer, J. M., Yeh, H. J. C., Liu, X., Yagi, H., Schurter, E., and Gorenstein, D. (1996) *Polycyclic Aromatic Compounds 10*, 145−152.

37. Zegar, I. S., Kim, S. J., Johansen, T. N., Horton, P. J., Harris, C. M., Harris, T. M., and Stone, M. P. (1996) *Biochemistry 35*, 6212−6224.
38. Sayer, J. M., Shah, J. H., Liang, C., Xie, G., Kroth, H., Yagi, H., Liu, X., Yeh, H. J. C., and Jerina, D. M. (1999) *Polycyclic Aromatic Compounds 17*, 95−104.
39. Cosman, M., Fiala, R., Hingerty, B. E., Laryea, A., Hongmee, L., Harvey, R. G., Amin, S., Geacintov, N. E., Broyde, S., and Patel, D. (1993) *Biochemistry 32*, 12488−12497.
40. Cosman, M., Laryea, A., Fiala, R., Hingerty, B. E., Amin, S., Geacintov, N. E., Broyde, S., and Patel, D. J. (1995) *Biochemistry 34*, 1295−1307.
41. Li, Z., Kim, H.-K., Tamura, P. J., Harris, C. M., Harris, T. M., and Stone, M. P. (1999) *Biochemistry 38*, 2969−2981.
42. Li, Z., Kim, H.-K., Tamura, P. J., Harris, C. M., Harris, T. M., and Stone, M. P. (1999) *Biochemistry 38*, 16045−16057.
43. Xu, R., Mao, B., Amin, S., Geactinov, N. E. (1998) *Biochemistry 37*, 769−778.

BI001669L